

The dynamics and scaling law for particles suspended in shear flow with inertia

By E-JIANG DING AND CYRUS K. AIDUN†

Institute of Paper Science and Technology, and George W. Woodruff School
of Mechanical Engineering at Georgia Institute of Technology 500 10th Street, N.W.,
Atlanta, GA 30318, USA

(Received 22 February 1999 and in revised form 16 May 2000)

The effect of inertia on the dynamics of a solid particle (a circular cylinder, an elliptical cylinder, and an ellipsoid) suspended in shear flow is studied by solving the discrete Boltzmann equation. At small Reynolds number, when inertia is negligible, the behaviour of the particle is in good agreement with the creeping flow solution showing periodic orbits. For an elliptical cylinder or an ellipsoid, the results show that by increasing the Reynolds number, the period of rotation increases, and eventually becomes infinitely large at a critical Reynolds number, Re_c . At Reynolds numbers above Re_c , the particle becomes stationary in a steady-state flow. It is found that the transition from a time-periodic to a steady state is through a saddle-node bifurcation, and, consequently, the period of oscillation near this transition is proportional to $|p-p_c|^{-1/2}$, where p is any parameter in the flow, such as the Reynolds number or the density ratio, which leads to this transition at $p = p_c$. This universal scaling law is presented along with the physics of the transition and the effect of the inertia and the solid-to-fluid density ratio on the dynamics. It is conjectured that this transition and the scaling law are independent of the particle shape (excluding *body of revolution*) or the shear profile.

1. Introduction

The motion and dynamics of a single particle suspended in simple shear flow is fundamental to understanding suspension hydrodynamics. The physics of such a system at negligible particle Reynolds number, when inertia can be totally neglected, has been studied extensively (Jeffery 1922; Bretherton 1961; Goldsmith & Mason 1961). Comprehensive review articles document significant progress in this area (Leal 1980; Bossis & Brady 1984; Brady & Bossis 1988). However, for finite particle Reynolds number, when inertia cannot be neglected, the dynamics of even the simplest case—a single particle suspended in Couette flow—is not known. In this study, the dynamics of a circular cylinder, an elliptical cylinder, and an ellipsoid suspended between two parallel plates in simple shear is investigated.

The motion of a circular cylinder freely suspended and placed symmetrically in a steady simple shear at small Reynolds number has been investigated by Robertson & Acrivos (1970). They have obtained the first-order correction term to the creeping-flow solution using the inner and outer asymptotic expansion. Kossack & Acrivos (1974) presented numerical solutions to the full two-dimensional Navier–Stokes equations for values of Re up to 280. They found that the dimensionless rotational speed of the freely suspended cylinder decreases as $Re^{-1/2}$ for high Reynolds number.

† Author to whom correspondence should be addressed.

Poe & Acrivos (1975) present experimental data for a rotating cylinder in a simple shear flow where three different confinement ratios of the channel width, H , to the radius, r , of the cylinder have been used. However, the influence of the confinement ratio on the values of the dimensionless rotation rate is not discussed. For low Reynolds number, their experimental results are in agreement with the results obtained numerically by Kossack & Acrivos (1974). Owing to the appearance of flow instabilities, steady flow experiments could not be performed for Re higher than 23.

Recently an experimental investigation was carried out in the range $39 \leq Re \leq 108$ by Zettner & Yoda (2000). In contrast to a stationary cylinder, in this case there is a layer of fluid moving with a freely rotating cylinder, and therefore the stagnation points are not on the surface of the cylinder. The locations of the stagnation point and the velocity field around the stationary as well as the rotating cylinder are measured using particle image velocimetry (PIV). In this range of Reynolds number, the $Re^{-1/2}$ relation concerning the dimensionless rotational speed of the freely suspended cylinder, predicted by numerical calculation (Kossack & Acrivos 1974), is not observed in the experiments. Besides, the rotation rate of the cylinder in steady state at $Re \approx 20$ obtained by Poe & Acrivos (1975) is considerably lower than the rate of rotation obtained by Zettner & Yoda (2000) at $Re \approx 39$. The reason for the discrepancy between the previous studies for a circular cylinder is explored and clarified in this paper as background information for the new results on the dynamics of elliptical cylinders and ellipsoids at high Re .

A thorough understanding of the behaviour of elliptical cylinders and ellipsoids freely suspended in a shear flow is fundamentally important for understanding and predicting flow behaviour in suspension rheology. In many flow problems, such as suspension flow in blade coating, the particle Reynolds number could be much larger than one. However, most of the effort in the past has been devoted to flows with negligible particle Reynolds number. The work described here presents a computational investigation of an elliptical cylinder and an ellipsoid freely suspended in a shear flow for values of particle Reynolds number from 0.08 up to 100. With small Reynolds number ($Re = 0.08$), results from computations for an elliptical cylinder in a shear flow show good agreement with the analytical solutions obtained by Jeffery (1922). When the Reynolds number is increased, it is found that inertia has a significant impact on the particle motion.

The motion of an elliptical cylinder and an ellipsoid suspended in a simple shear flow at zero Reynolds number is well understood. Analytical solutions for two special cases were discussed by Jeffery (1922). Assume that (x', y', z') are coordinates fixed in space, and that the shear flow is $(u, v, w) = (0, 0, -Gy')$, where G is the shear rate and the vorticity vector is parallel to the x' -axis. Jeffery (1922) studied the motion of a solid ellipsoid, given by

$$\frac{x'^2}{a^2} + \frac{y'^2}{b^2} + \frac{z'^2}{c^2} = 1 \quad (1)$$

in a simple shear flow at vanishing Reynolds number. He assumed the force and torque on the particle to be zero. One of the special cases is when one of the principal axes, say x , of the ellipsoid is kept parallel to the vorticity vector in the shear flow with the ellipsoid rotating around this axis. The angle and the angular rate are given by

$$\chi = \tan^{-1} \left(\frac{b}{c} \tan \frac{bcGt}{b^2 + c^2} \right), \quad (2)$$

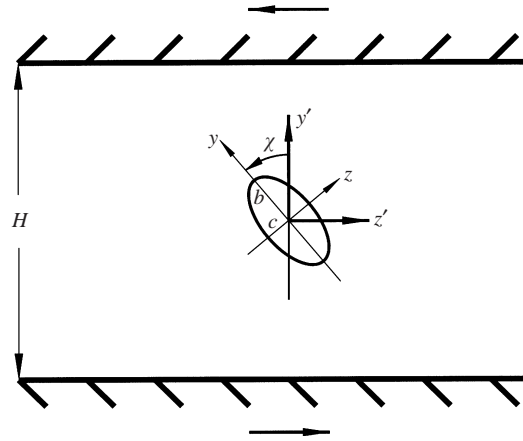


FIGURE 1. Computational domain for the rotation of an elliptical cylinder in a simple shear flow. This elliptical cylinder is a limiting case of the ellipsoid $x^2/a^2 + y^2/b^2 + z^2/c^2 = 1$ with $1/a \rightarrow 0$. (x', y', z') are coordinates fixed in space, where the x' -axis is parallel to the vorticity vector. The shear flow is $(u, v, w) = (0, 0, -Gy')$. (x, y, z) are coordinates fixed on the elliptical cylinder, where the x -axis is parallel to x' . χ is the angle from the y' -axis to the y -axis, i.e. the orientation of the elliptical cylinder.

$$\dot{\chi} = \frac{G}{b^2 + c^2} (b^2 \cos^2 \chi + c^2 \sin^2 \chi), \quad (3)$$

where t represents time; χ and $\dot{\chi}$ are the angle and the angular rate of the rotation, respectively. In this problem, one of the ellipsoid's principal axes, x , is always parallel to x' . This solution also applies to a two-dimensional ellipse, or an elliptical cylinder (as shown in figure 1), an ellipsoid with one principal axis, a , extended to infinity. From the above analytical solution, it is clear that the motion of the ellipsoid or ellipse is periodic with the period

$$T = \frac{2\pi(b^2 + c^2)}{bcG}. \quad (4)$$

In every time interval, T , the particle completes a full rotation. For a circular cylinder, $b = c = r$, the angular rate of rotation is steady in time, and the period is $T = 4\pi/G$.

From Jeffery's solution, (2) and (3), the question one may ask is how the motion of the ellipse or the ellipsoid will be influenced by the presence of inertia, that is when the particle Reynolds number is not zero. Feng & Joseph (1995) calculated this special two-dimensional case with finite Reynolds number ($Re = 1.0$ in their calculation) by a quasi-steady approximation and confirmed that with small Reynolds number the motion of the particle is only slightly influenced. They concluded that the moment of inertia of the ellipse has a weak effect on its rotation at small Reynolds number. However, it has been found that as the Reynolds number is increased, the motion of the particle will be dominated by inertia, and a new state will appear at a critical Reynolds number (Aidun & Ding 1997; Aidun, Lu & Ding 1998). In the present paper, this transition has been analysed and generalized through a universal scaling law.

The computational method used in the present work is based on the solution of the discrete Boltzmann equation to determine the motion of particles suspended in fluid (McNamara & Zanetti 1988; Ladd 1994*a, b*, 1996, 1997; Aidun & Lu 1995; Aidun, Lu & Ding 1997, 1998). In this method, the fluid is described by the discrete version of Boltzmann equation while the motion of the solid particle is determined by the Newtonian dynamics equation. The application of the lattice-Boltzmann method to the motion of solid particles suspended in fluid was first suggested by Ladd (1994*a, b*).

Ladd's method, requiring the fluid to occupy the entire computational domain, can only be used to simulate solid particles with density larger than that of fluid. A method without this limitation is presented by Aidun *et al.* (1998) along with several examples demonstrating its accuracy and robustness.

The purpose of the present work is to provide a better understanding of the effect of inertia on particle dynamics in shear flow. Section 2 presents the basic equations for the motion of the solid particle suspended in fluid, along with dimensional analysis. Section 3 outlines the results from simulation of a circular cylinder in a simple shear flow with small and moderate values of Reynolds number. At small Reynolds numbers the results presented in this paper are in agreement with the experiments by Poe & Acrivos (1975), while at moderate Reynolds numbers they are in good agreement with experiments by Zettner & Yoda (2000). The confinement ratio H/r has been proven to play an important role in determining the rotating rate of the cylinder at steady state. In §4, the motion of an elliptical cylinder in a simple shear flow is discussed. In this study, the problem is examined with Reynolds number increasing from 0 to 50. The results show that as the Reynolds number increases, the period of rotation, T , increases to infinity at a critical point, where $Re = Re_c$, beyond which ($Re > Re_c$) the particle becomes stationary in a steady-state shear flow. In §5, it is shown that the critical value Re_c depends on another important dimensionless parameter, the solid-to-fluid density ratio, $\alpha = \rho_s/\rho_f$. The motion of an ellipsoid in shear flow is discussed in §6. Results in this paper are summarized in §7. Some conclusions and hypotheses are presented in §8.

2. Dimensional analysis

The equations for particle motion in a Newtonian fluid, that is, the usual Navier–Stokes and continuity equations complemented by the Newtonian Dynamics equation govern the motion of the solid particle. In non-dimensional form, these equations are given by

$$Re \left(\frac{\partial \mathbf{u}}{\partial t} + \mathbf{u} \cdot \nabla \mathbf{u} \right) = -\nabla p + \nabla^2 \mathbf{u}, \quad (5)$$

$$\nabla \cdot \mathbf{u} = 0, \quad (6)$$

$$\alpha q Re \frac{d^2 \chi}{dt^2} = N, \quad (7)$$

where N is the sum of torques on the particle about the x -axis. In these equations, length, velocity, time, and torque are scaled by d , Gd , $1/G$, and μGd^n , respectively, where d is an appropriate particle length scale, such as $2b$ for an ellipse. For two-dimensional cases, inertia and torque are per unit length, and therefore, $n = 2$; for three-dimensional cases, $n = 3$. There are three parameters in this equation that influence the flow. These are the Reynolds number, $Re = \rho_f Gd^2/\mu$, the solid-to-fluid density ratio, $\alpha = \rho_s/\rho_f$, and the shape parameter, $q = I/\rho_s d^{n+2}$, where I is the moment of inertia of the solid particle about the x -axis. In this paper we only discuss the effect of the first two parameters, Re and α , on the motion of the particle.

The quasi-steady approximation for particle motion used in Stokes flow approximations (Feng & Joseph 1995) given by

$$\nabla p = \nabla^2 \mathbf{u}, \quad \nabla \cdot \mathbf{u} = 0, \quad N = 0,$$

neglects the fluid as well as the solid inertia. The computational results presented

below are obtained by including all of the inertia and viscous terms regardless of the value of Re .

In this study, the recently developed lattice-Boltzmann method (Aidun *et al.* 1998) is used for dynamical analysis of particles suspended in fluid. The fluid is modelled by a group of fluid particles moving in a cubic lattice with discrete velocities. These fluid particles are either at rest, or moving along the lattice links. The lattice-Boltzmann equation describing the motion of the fluid particles is written as

$$f_{\sigma i}(\mathbf{x} + \mathbf{e}_{\sigma i}, t + 1) - f_{\sigma i}(\mathbf{x}, t) = -\frac{1}{\tau} [f_{\sigma i}(\mathbf{x}, t) - f_{\sigma i}^{(0)}(\mathbf{x}, t)], \quad (8)$$

where $f_{\sigma i}(\mathbf{x}, t)$ is the single-particle distribution function, $f_{\sigma i}^{(0)}(\mathbf{x}, t)$ is the equilibrium distribution at (\mathbf{x}, t) , and τ is the single relaxation time. For the present model, the speed of sound is $c_s = \sqrt{1/3}$, and the kinematic viscosity is $\nu = (2\tau - 1)/6$. The solid particle, however, moves in a continuous way, based on the Newtonian dynamics. The position of the solid particle is updated by a fourth-order Runge–Kutta solution of the Newtonian dynamical equation. The interaction between fluid and solid particle is calculated by the ‘no-slip’ rule. Detailed discussion of the interaction and the motion of solid particles can be found in an earlier publication (Aidun *et al.* 1998).

Since the surface of the particle is projected on a discrete computation lattice, the particle boundary is defined by connected straight lines. As discussed previously (Aidun *et al.* 1998), the boundary is always assumed to be at the midpoint of the boundary nodes when the interaction between solid particle and fluid is considered. When the method is used to simulate a system with high solid particle concentration, relatively few computational lattices are used to outline the particle. In that case, an effective hydrodynamic radius, r_a , for sphere is defined by calculating the drag coefficient of a sphere (Ladd 1994*b*), where r_a depends on the kinematic viscosity, ν . In the present study, however, there is only a single solid particle in a simple shear flow, and the radius of the solid particle varies from 8 to 64 in different cases; therefore, the influence of viscosity on the ‘effective hydrodynamic dimension’ is negligible. Moreover, the ‘effective hydrodynamic dimension’ of an ellipse or ellipsoid so defined has not been studied yet. Hence, the effective hydrodynamic radius is simply replaced by the real radius, r . To test the validity of this approach, a circular cylinder rotating in a simple shear flow is analysed for a wide range of kinematic viscosities. The computational domain is 278×32 lattice units, and the radius, r , of the cylinder is 7.99 lattice units. At Reynolds number, $Re = 3.192$, the value of ν varies from 1/4 to 1/64. It is found that for particles of such large size, the value of the kinematic viscosity, when less than 1/4, has an insignificant influence on the results. In fact, the dimensionless rotation rate, $\dot{\chi}/G$, remains constant for all values of ν for steady and transient states. Therefore, in the present study the influence of kinematic viscosity on the effective hydrodynamic radius will be neglected.

3. A circular cylinder in a simple shear flow

A thorough investigation of the behaviour of a circular cylinder freely suspended in simple shear flow is essential to the understanding of many complex problems in suspension hydrodynamics. The present study is focused on the angular velocity and streamline patterns for a circular cylinder suspended in a simple shear flow. The Reynolds number covers the range up to about 320. Results are summarized in figure 2.

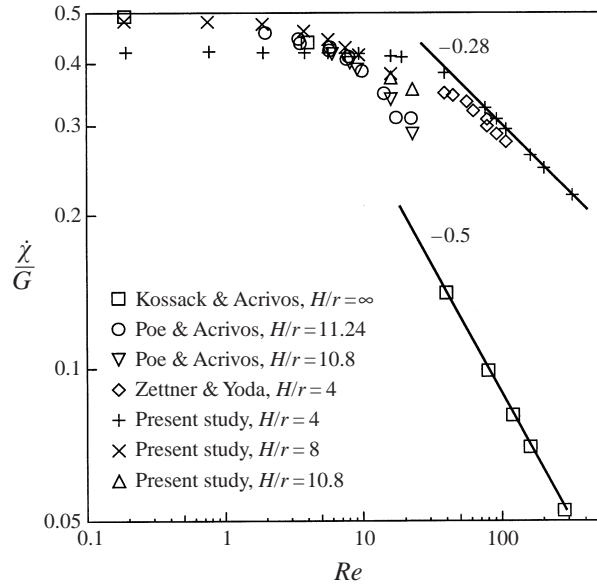


FIGURE 2. Comparison of the simulation results on the angular rate of rotation of a circular cylinder in shear flow with other numerical and experimental results. The angular rates obtained in numerical simulation are always larger than the corresponding data obtained in experiments. The numerical results obtained by Kossack & Acrivos (1974) at high Reynolds number can be fitted by a straight line with slope = -0.5 . The results for $H/r = 4$ by the present simulation, however, are fitted by a straight line with slope = -0.28 .

For very low Reynolds number, where inertia can be neglected, the angular rate of rotation of the cylinder is given by (3), $\dot{\chi} = G/2$. Results from simulations of a freely suspended circular cylinder in a simple shear flow with $Re = 0.08$ are obtained. In this simulation, the computational domain includes $L \times H = 640 \times 320$ lattice nodes, the fluid viscosity $\nu = 0.5$, the density ratio $\alpha = \rho_s/\rho_f = 1.0$, and the radius of the circular cylinder $r = 16$ lattice nodes. The dimensionless rotation rate reaches steady state at $\dot{\chi}/G = 0.4982$, in good agreement with the value of 0.5 predicted by (3) for $Re = 0$. As predicted by Kossack & Acrivos (1974), when the value of the Reynolds number increases, the dimensionless angular rate of rotation, $\dot{\chi}/G$, decreases in value. However, it should also be noted that the rotation rate of the cylinder at the steady state is dependent on the confinement ratio H/r . In the above simulation, the confinement ratio, H/r , is 20. When $H/r = 8$, the rotation rate is 0.4820 at $Re = 0.187$. When H/r decreases to 4, the rotation rate is 0.4192 at $Re = 0.192$. The asymptotic expansion obtained by Kossack & Acrivos (1974) is for a free boundary condition, corresponding to $H/r \rightarrow \infty$. For small Reynolds numbers the dimensionless rotation rate of the cylinder at steady state decreases when the width of the channel decreases.

It is also found that the dimensionless rotation rate, $\dot{\chi}/G$, reaches a plateau at low Reynolds number. When $H/r = 8$, $\dot{\chi}/G$ is found to be about 0.48 for $Re \leq 3$. When $H/r = 4$, the value of $\dot{\chi}/G$ is about 0.42 for $Re \leq 9$. For an infinitely large system where $H/r \rightarrow \infty$ the maximum value of $\dot{\chi}/G$ is 0.5, according to (3). The existence of the two parallel solid walls in the system suppresses the maximum value of $\dot{\chi}/G$ to values lower than 0.5. In the paper by Poe & Acrivos (1975), the data from a cylinder suspended in shear flow are not provided for very low Reynolds number, and therefore the plateau is missing from the results in their experiments.

For higher Reynolds numbers, $6 \leq Re \leq 20$, the present computational results are compared to the experiments by Poe & Acrivos (1975). Confinement ratio was taken to be $H/r = 6.32, 10.8, \text{ or } 11.24$ in the experiments, while the rotating rate of the cylinder at the steady state did not strongly depend on the confinement. In the present calculation $H/r = 8$ is chosen. The results of the present computation are in good agreement with the experiments by Poe & Acrivos (1975), as shown in figure 2.

For Reynolds numbers above 20, the present computational analysis deviates from the experiments by Poe & Acrivos (1975). The experiments show that $\dot{\chi}/G = 0.311$ (when $Re = 22.4$ and $H/r = 11.24$), $\dot{\chi}/G = 0.290$ (when $Re = 22.96$ and $H/r = 10.8$), and $\dot{\chi}/G = 0.309$ (when $Re = 22.44$ and $H/r = 6.32$). However, in the present calculation the rotating rate is $\dot{\chi}/G = 0.3545$ (when $Re = 22.96$ and $H/r = 10.8$), apparently higher than the experimental results. In the experiments (Poe & Acrivos 1975) when the Reynolds number is higher than 23 the shear flow becomes unstable. The shear flow instability in the experiments might lead to dissipation of the kinematic energy, and lower the rotating rate of the cylinder. The present computational method being in two-dimensions, however, is not able to capture the instability in the experiments.

Recently, experiments at moderate Reynolds numbers, $39 \leq Re \leq 108$, were carried out by Zettner & Yoda (2000). In order to compare the present computational results with the experiments in this range of Reynolds numbers, the size of the computational domain is for the moment fixed at 2224×256 lattice nodes, and the radius of the circular cylinder is $r = 64$ lattice nodes. The time relaxation parameter used in the discrete Boltzmann equation is taken to be $\tau = 1.0$, or $\nu = 1/6$. The solid-to-fluid density ratio is $\alpha = \rho_s/\rho_f = 1$. The confinement and the density ratio are in agreement with the experimental setup of Zettner & Yoda (2000). Comparing the results obtained by Poe & Acrivos (1975) and those by Zettner & Yoda (2000), they do not seem to be in agreement as the rotating rate of the cylinder at the lower Reynolds number of about 20 (Poe & Acrivos 1975) is even lower than that at the higher Reynolds number of about 39 (Zettner & Yoda 2000). The present investigation shows that the rotating rate of the cylinder at steady state strongly depends on the confinement ratio H/r at Reynolds number in the range of $20 < Re < 40$. This explains the discrepancy between the two experiments.

When a cylinder suspends freely in between two parallel plates moving in opposite directions, simulations give results in relatively good agreement with the experimental results by Zettner & Yoda (2000). Comparison of the computational results with the experiments presented in figure 2 shows a difference in rate of rotation of about 9% at $Re = 39$ and 5% at $Re = 108$. To verify the accuracy of the computational method, the results for a freely suspended cylinder at $Re = 39.168$ are obtained with five different computational parameters, namely $(\tau, r) = (1.0, 64), (0.625, 32), (0.5625, 16), (0.75, 16), \text{ and } (0.5625, 8)$. The dimensionless rotating rate at steady state is found to be 0.3816, 0.3829, 0.3796, 0.3790, and 0.3790, respectively. Different values of the relaxation parameter and various sizes of the computational domain yield very close results, showing the independence of the results from the number of computational lattices and the relaxation parameter, τ . The simulation results are always larger than those of the experiments, which suggests that this discrepancy may be due to a small amount of friction at the two ends of the cylinder in the experiments.

The streamlines around a freely rotating circular cylinder at Reynolds number $Re = 76.8$ presented in figure 3. A similar pattern is obtained in the experiments by Zettner & Yoda (2000). It is clear that flow near the moving walls contributes a positive torque in favour of the particle rotation, while the recirculating flow in the central region in between the two plates exerts a negative torque (i.e. in a direction

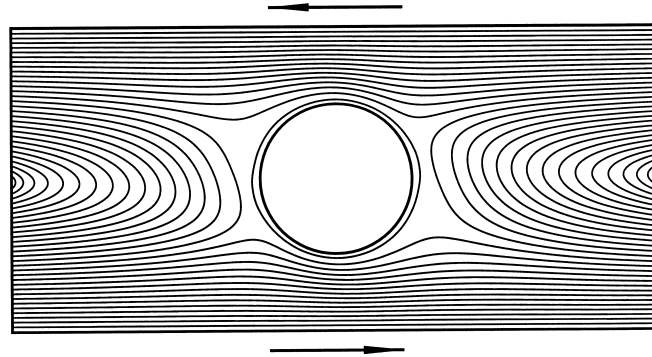


FIGURE 3. The streamlines for a freely rotating circular cylinder in shear flow. The Reynolds number is $Re = 76.8$. A similar pattern is observed in experiment.

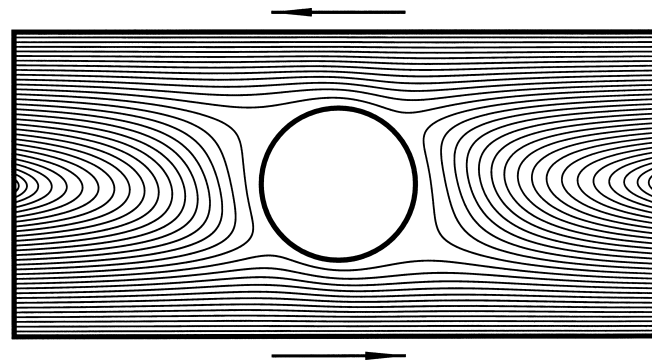


FIGURE 4. The streamlines for a fixed circular cylinder in shear flow. The Reynolds number is $Re = 76.8$.

resisting the rotation of the cylinder) on the cylinder. This unfavourable contribution to the torque increases with the Reynolds number, reducing the frequency of rotation of the cylinder. A third region is the confined flow pattern (i.e. closed streamlines) moving near and around the cylinder due to the no-slip condition at the surface. This layer obviously transfers the momentum from the moving walls and the recirculating flow to the cylinder. The net effect of the liquid layer around the cylinder is a small amount of drag reducing the rate of rotation.

As a reference, the streamlines from the computational results at $Re = 76.8$ for a fixed cylinder are presented in figure 4. The main qualitative difference with a freely moving cylinder is the absence of the closed layer around the cylinder and the attachment of the four separation points on the surface of the cylinder. The computed downstream and upstream stagnation points on the top half of the circular cylinder are located at $+43.4^\circ$ and -49.7° from the y' -axis, respectively.

In both cases of a freely moving or a fixed cylinder, as the Reynolds number increases, the upstream and downstream stagnation points move closer to each other and the magnitude of the negative torque on the cylinder from the recirculating region increases.

The components w (in the z' -direction) and v (in the y' -direction) of the velocity profile at some sections in the computational domain are compared with the experimental measurements by Zettner & Yoda. Figure 5(a) shows the comparison for

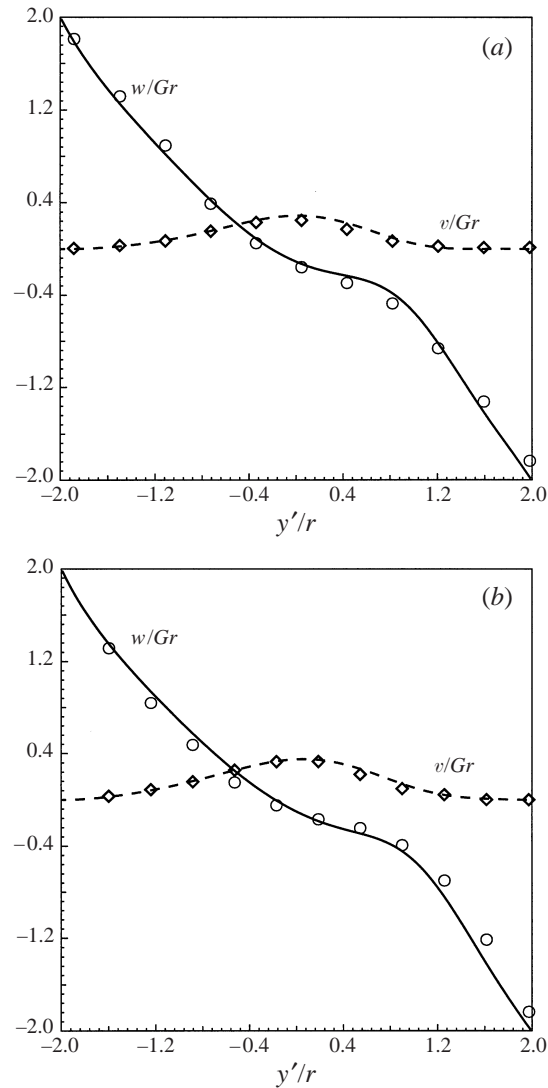


FIGURE 5. (a) The velocity components w and v versus y' for a rotating cylinder at section $z'/r = -1.8467742$. The Reynolds number is $Re = 79.6$. (b) The velocity component v versus y' for fixed cylinder at section $z'/r = -1.875$. The Reynolds number is $Re = 76.8$. The symbol \circ represents w/Gr in the experimental data, while solid line represents simulation results. The symbol \diamond represents v/Gr in the experimental data, while dashed line represents simulation results.

a rotating cylinder, and figure 5(b) for a fixed cylinder, at a selected section. The computational results show good agreement with the data.

For high Reynolds number, the theoretical investigation by Kossack & Acrivos (1974) predicted a scaling relation showing that the rotation rate decreases as $Re^{-1/2}$. In order to examine the scaling relation for the rotation rate for high Reynolds number, the simulation is extended to Reynolds numbers up to $Re = 320$ for $H/r = 4$. The $-1/2$ exponent, however, is not found in the present study. With $H/r = 4$ the rotation rate can be approximated by a power law with exponent -0.28 . As shown in figure 2, the data obtained in the experiments with $H/r = 4$ by Zettner & Yoda (2000)

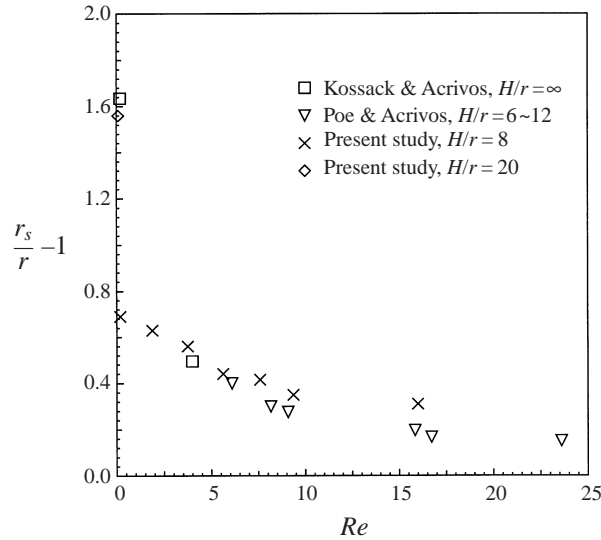


FIGURE 6. Location of the stagnation point for a freely rotating cylinder in a simple shear. r_s is the distance between the stagnation point and the centre of the circular cylinder.

follow the same scaling behaviour with exponent close to -0.28 . The $-1/2$ scaling law by Kossack & Acrivos is not observed by the present computational investigation or by Zettner & Yoda's experiments using the confined channel with $H/r = 4$. Since the exponent, $-1/2$, in the scaling relation, found by Kossack & Acrivos (1974) for a circular cylinder, depends on the confinement of the channel, it is not universal.

The location of the stagnation point computed for the rotating cylinder is calculated and compared with numerical results (Kossack & Acrivos 1974) as well as experimental data (Poe & Acrivos 1975). Results are summarized in figure 6. The distance r_s from a stagnation point to the centre of the cylinder depends on the Reynolds number as well as the confinement ratio, H/r . At very low Reynolds numbers the results obtained at $H/r = 8$ are much lower than the numerical results by Kossack & Acrivos (1974). The discrepancy can be explained by the fact that the method of Kossack & Acrivos is based on an unbound large system. When the confinement ratio increases to $H/r = 20$, however, the results obtained by the present calculation are in good agreement with the numerical results by Kossack & Acrivos (1974). At Reynolds number between 5 and 10, with $H/r = 8$ the results by the present method are in good agreement with the experiments by Poe & Acrivos (1975). However, for Reynolds number above 15, the present calculation results are higher than the experimental data. When $H/r = 4$ the location of the stagnation point at various Reynolds numbers is provided in table 1.

4. The effect of Reynolds number on the dynamics of an elliptical cylinder

In this section, we present and discuss the effect of inertia on the dynamics of a neutrally buoyant (i.e. $\alpha = \rho_s/\rho_f = 1.0$) elliptical cylinder in shear flow. The effect of the density ratio on the dynamics will be discussed in the next section.

Results from a simulation of a freely suspended elliptical cylinder in simple shear flow with $Re = Gd^2/\nu = 0.08$, where the major axis $b = 2c$, have been presented before (Aidun *et al.* 1998). The computational results are in good agreement with

Reynolds number	Stagnation point
0.768	$(\pm 0.008r, \pm 1.281r)$
39.168	$(\pm 0.148r, \pm 1.203r)$
76.8	$(\pm 0.195r, \pm 1.125r)$
93.04	$(\pm 0.242r, \pm 1.094r)$
108.54	$(\pm 0.242r, \pm 1.078r)$

TABLE 1. The location of the stagnation points (y', z') for the rotating circular cylinder when $H/r = 4$.

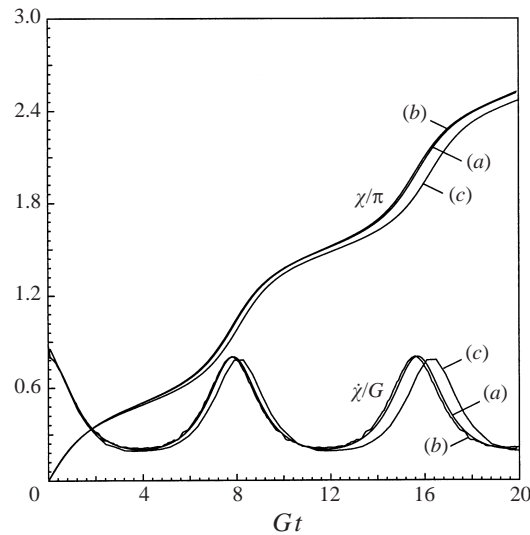


FIGURE 7. Orientation and rate of rotation of an ellipse at small particle Reynolds number. (a) Jeffery's solution for $Re = 0$; (b) computational result at $Re = 0.08$; and (c) computational result at $Re = 1.0$.

Jeffery's solution, as shown in figure 7. As the Reynolds number approaches 1.0, the results deviate from the asymptotic solution with a larger period of rotation.

When the Reynolds number is large, the behaviour of the system becomes quite different from Jeffery's solution. In the remaining part of this section, the computational grid system size is 1600×320 , the ellipse's size is $b = 32$ and $c = 16$, and the shear rate is $G = 1/2048$. The fluid viscosity is adjusted for computations at Reynolds number $Re = 5, 10, 15, 20, 24, 26, 28, 30, 40$ and 50 . The rates of rotation of the particle at various Re are shown in figure 8. When $Re \leq 28$, the motion of the ellipse is a periodic rotation with non-uniform angular velocity. At larger Reynolds number, $Re \geq 30$, however, the ellipse does not rotate any longer; instead it takes a stationary position in the shear field (Aidun & Ding 1997).

The minimum of $\dot{\chi}/G$ decreases as the Reynolds number increases, as shown in figure 9 with a straight line fit, given by

$$\frac{\dot{\chi}_{min}}{G} \sim Re_c - Re, \quad (9)$$

where $Re_c \simeq 29$ is a critical Reynolds number. The period of the rotation increases rapidly as the Reynolds number becomes larger, as shown in figure 10. Denote

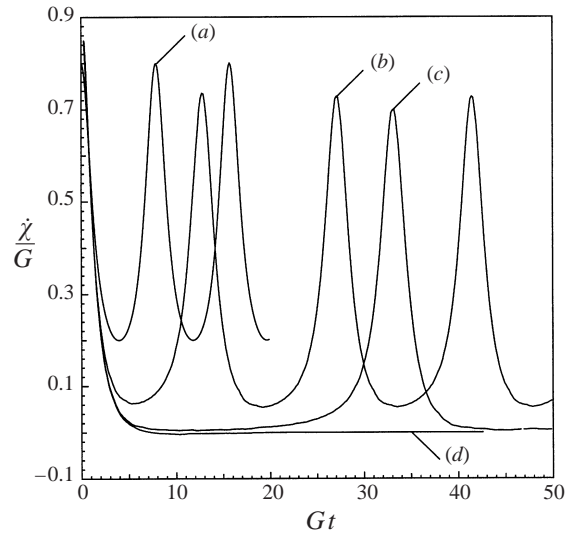


FIGURE 8. The rate of rotation of an elliptical cylinder in a shear field between two parallel channels at various particle Reynolds numbers. (a) $Re = 0$; (b) $Re = 15$; (c) $Re = 28$; and (d) $Re = 30$. These results show the lack of existence of the periodic state at $Re \geq 30$.

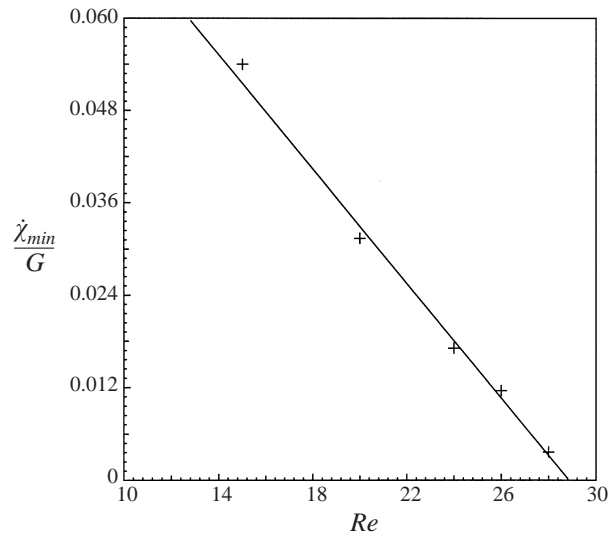


FIGURE 9. The minimum of the angular velocity decreases as Reynolds number increases. The straight line is the best fit to the simulation results. At $Re_c \sim 29$ the minimum of the angular rate is expected to vanish.

$\epsilon = \dot{\chi}_{min}/G$, and χ_0 as the angle at which the ellipse has its minimum angular velocity. Since $\dot{\chi}$ reaches its minimum at $\chi = \chi_0$, it can be expanded in the vicinity of χ_0 as

$$\frac{\dot{\chi}}{G} \sim \epsilon + A(\chi - \chi_0)^2, \quad (10)$$

where A is a positive constant. The period T is basically dependent on the length of

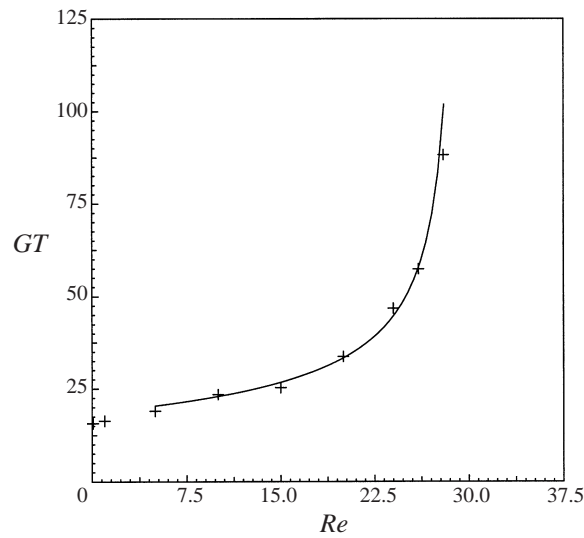


FIGURE 10. The period of the motion of the ellipse increases to infinity as the Reynolds number goes to the critical value. The curve in the figure presents equation (12) with $C = 100$ and $Re_c = 29$, which is in good agreement with the simulation results.

time the ellipse is oriented in the vicinity of χ_0 , hence

$$T \sim \int_{\chi_1}^{\chi_2} \frac{d\chi}{\dot{\chi}} \quad (11)$$

where $\chi_1 < \chi_0$ and $\chi_2 > \chi_0$ are two constants, independent of ϵ . With the application of (10) near the transition point, that is where $\epsilon \rightarrow 0$, it is found that $T \sim \epsilon^{-1/2}$, or

$$GT = C(Re_c - Re)^{-1/2}, \quad (12)$$

where C is a constant. For the ellipse considered here with critical Reynolds number, $Re_c = 29$, the constant value, $C = 100$, provides a very good prediction of the results as shown in figure 10.

It is easy to see that χ_0 , the angle at which the ellipse has its minimum angular velocity, is exactly $\pi/2$ when $Re = 0$. However, when $Re > 0$ the angle χ_0 is always smaller than $\pi/2$. In fact, $\chi_0 \simeq 0.476\pi$ when $Re = 1$, and $\chi_0 \simeq 0.45\pi$ when $Re = 28$. Moreover, when $Re > Re_c$, the angle of the ellipse corresponding to the stable stationary orientation decreases as Re increases. For example, when $Re = 50$ the stable angle is about 0.37π , smaller than the orientation angle at the critical Reynolds number.

To better understand the physical behaviour of the problem and the transition of the system from periodic to steady state at the critical Reynolds number, the streamlines at different values of Re are examined. To examine the forces on the particle, the net torque on a fixed particle in shear flow is computed. The streamlines for the system with orientation angle $\chi = (4/9)\pi = 80^\circ$ are shown in figure 11. There are two groups of streamlines in figure 11(a): the shear layer close to the walls and the recirculation region at the centre. The shear layer contributes a positive torque on the particle while the recirculating region of the fluid has a negative contribution. The net torque on the particle is dependent on the particle Reynolds number. For an ellipse where $c < b$, the net torque on the particle is dependent also on the orientation

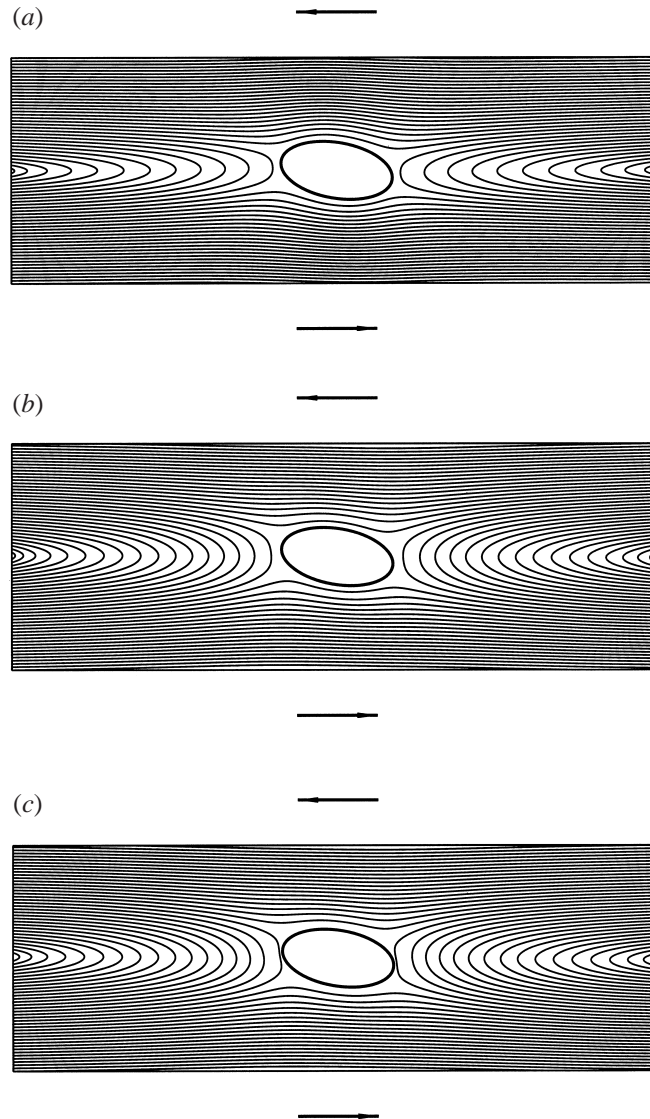


FIGURE 11. The streamlines when the ellipse is fixed in shear flow with the orientation angle $\chi = 80^\circ$. (a) $Re = 1$, (b) $Re = 20$, (c) $Re = 40$.

of the particle. The streamlines at particle Reynolds numbers $Re = 1$, 20, and 40, are shown in figures 11(a) to 11(c), respectively. The larger the Reynolds number, the larger the recirculation region of the flow. At $Re = 40$, the net torque on the solid particle is negative. If the particle is released in this case it will initially rotate in a clockwise manner before reaching the stationary orientation.

The computations for a fixed ellipse are extended to angles ranging between 0 and π , and the results are presented in figure 12. When $Re = 1$ or $Re = 20$ the torque on the solid particle is always positive, hence the solid particle rotates with the shear layer. When $Re = 40$, however, there are two points on the curve, the fixed points, where the net torque on the particle is zero. The fixed point at the smaller angle, $\chi = \chi_a$, is a stable fixed point. That is, if the initial angle is smaller than χ_a , the net

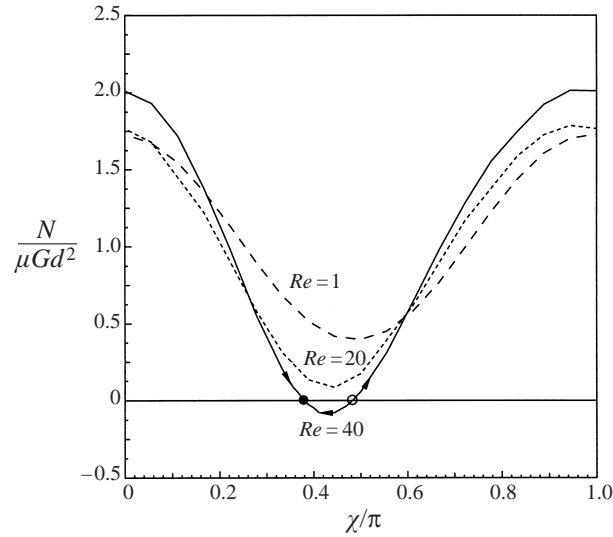


FIGURE 12. The net torque exerted on the ellipse by the fluid varies when the orientation angle changes. When $Re > Re_c$, the curve has two intersection points with the χ -axis. The left one, shown with a solid circle, is stable, while the right one, the open circle, is unstable. These points correspond to the stable (solid circle) and unstable (open circle) states in the phase-space trajectories shown in figure 14(c).

torque on the particle will be positive and the particle will rotate counter-clockwise; however, if the initial angle is larger than χ_a , the particle will rotate in a clockwise manner. In any case, the orientation of the particle will converge to the fixed point at $\chi = \chi_a$. On the other hand, the fixed point with larger angle, $\chi = \chi_b$, is unstable. That is, if the initial orientation is slightly disturbed near the fixed point χ_b , the particle will rotate to diverge away from the unstable fixed point and converge to the stable orientation. Then at transition, there must be a critical value of Reynolds number, Re_c , between 20 and 40 where the curve is just tangent to the χ -axis so that there is only one critical point. In fact, according to the results obtained above, it is clear that the critical value Re_c is about 29. The system undergoes a saddle-node bifurcation as the Reynolds number crosses the critical value. This explains the $-1/2$ exponent in the scaling law presented in (12), since the period of oscillation scales to this exponent for any saddle-node bifurcation (Lichtenberg & Lieberman 1992). The consequences of this finding in terms of the generality of the scaling will be presented in the following sections.

The information obtained in the simulation can be used to provide the distribution of the torque exerted by the fluid on the solid particle. The force $d\mathbf{f}$ on the segment dl on the edge of the ellipse is

$$d\mathbf{f} = \mathbf{S} \cdot \mathbf{n} dl, \quad (13)$$

where \mathbf{S} is the momentum flux tensor, and \mathbf{n} is the unit vector normal to the segment, as shown in figure 13(a). Then the torque at this segment is given by

$$dN = \mathbf{r} \times d\mathbf{f} = \mathbf{r} \times (\mathbf{S} \cdot \mathbf{n}) dl, \quad (14)$$

where \mathbf{r} is the vector from the mass centre of the particle to the segment dl . As the shear rate $G \rightarrow 0$, the momentum flux \mathbf{S} will be $\mathbf{S}^{(0)} = -p_0 \mathbf{I}$, where \mathbf{I} is the unit tensor, and p_0 is the pressure, which is a constant independent of position and time.

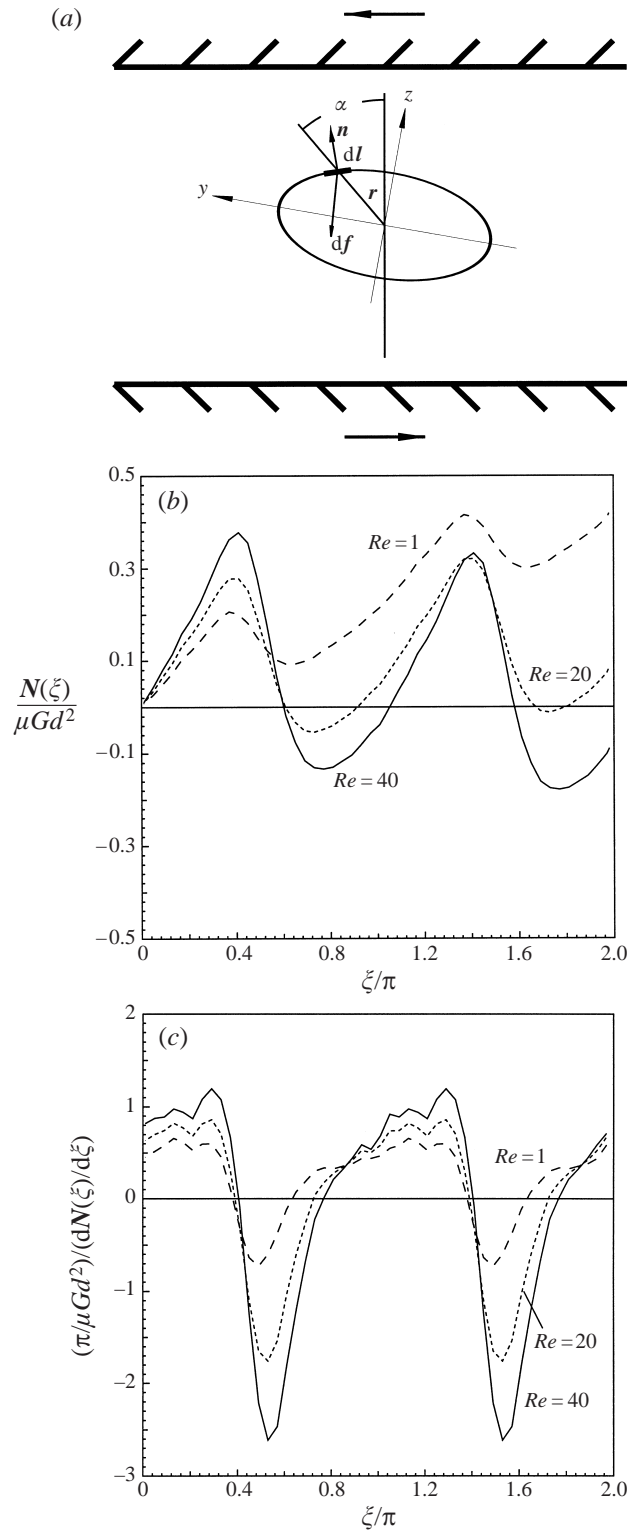


FIGURE 13. For caption see facing page.

Letting

$$\mathbf{S} = \mathbf{S}^{(0)} + \Delta\mathbf{S}, \quad (15)$$

since the first term $\mathbf{S}^{(0)}$ has no contribution on the net torque, N is given by

$$N = \int_0^{2\pi} \mathbf{r} \times (\mathbf{S} \cdot \mathbf{n}) \frac{dl}{d\xi} d\xi = \int_0^{2\pi} \mathbf{r} \times (\Delta\mathbf{S} \cdot \mathbf{n}) \frac{dl}{d\xi} d\xi. \quad (16)$$

Denoting

$$N(\xi) = \int_0^\xi \mathbf{r} \times (\Delta\mathbf{S} \cdot \mathbf{n}) \frac{dl}{d\xi} d\xi$$

then

$$\frac{dN(\xi)}{d\xi} = \mathbf{r} \times (\Delta\mathbf{S} \cdot \mathbf{n}) \frac{dl}{d\xi}.$$

With this method, one can calculate not only the total torque on the particle but also the angular distribution of the torque.

In the numerical simulation, the net torque is computed by contributions from the fluid nodes around the solid particle. The accumulation of the torque from $\xi = 0$ to 2π is shown in figure 13(b), and the torque distribution around the particle is shown in figure 13(c) for $Re = 1, 20$, and 40 . The results demonstrate the impact of inertia on the effect of forces due to fluid–solid interaction.

To investigate the mechanism of transition and to understand the physics of the particle behaviour, we examine the trajectories in the phase-space spanned by the orientation angle χ and its differential $d\chi/dt$. These trajectories for Reynolds number $Re = 20$ (sub-critical case), $Re = Re_c$ (the critical case), and $Re = 100$ (super-critical case) are shown in figures 14(a) to 14(c), respectively. The solid lines in these figures are obtained by computational simulation, while the dashed lines are drawn based on our knowledge of the dynamical behaviour of the system. In this numerical calculation, the transient process is omitted by cutting off the first several hundred time steps. The flow of the solution in the phase-space clearly shows a saddle-node bifurcation at the critical Reynolds number. The influence of the recirculation region on the net torque and the mechanism of transition, that is the type of bifurcation in the system dynamics, provide the key information in understanding the effect of inertia on the behaviour of a solid particle suspended in shear. Additional information and conclusions are presented in the following sections.

In order to verify the size of the computational grid used in these calculations, it is interesting to examine the effect of the grid size on the results. The results at $Re = 28$ and $Re = 30$ computed with 3200×640 and 1600×320 grid systems of lattice nodes are presented in figure 15. There is no qualitative difference between the results from the two grid systems. The only difference is quantitative; for example, the value of ϵ , the minimum of $\dot{\chi}/G$, for $Re = 28$ increases from 0.00367 to 0.00376 , and the predicted period of the rotation increases from $82.4/G$ to $88.2/G$. The small deviation in the period is caused by the inaccuracy in calculation of the angular rate of rotation. Since the rotation period, T , is proportional to $\epsilon^{-1/2}$, even a small error in ϵ , caused by the discretization of the solid surface, will result in a large deviation

FIGURE 13. (a) Notation used in the investigation of the angle distribution of the torque. (y', z') are coordinates fixed in space, while (y, z) are coordinates fixed on the ellipse. (b) The accumulated torque $N(\xi)$ versus ξ , the values of the torque at $\xi/\pi = 2.0$ are the net torque on the ellipse. (c) The torque per unit angle $dN(\xi)/d\xi$.

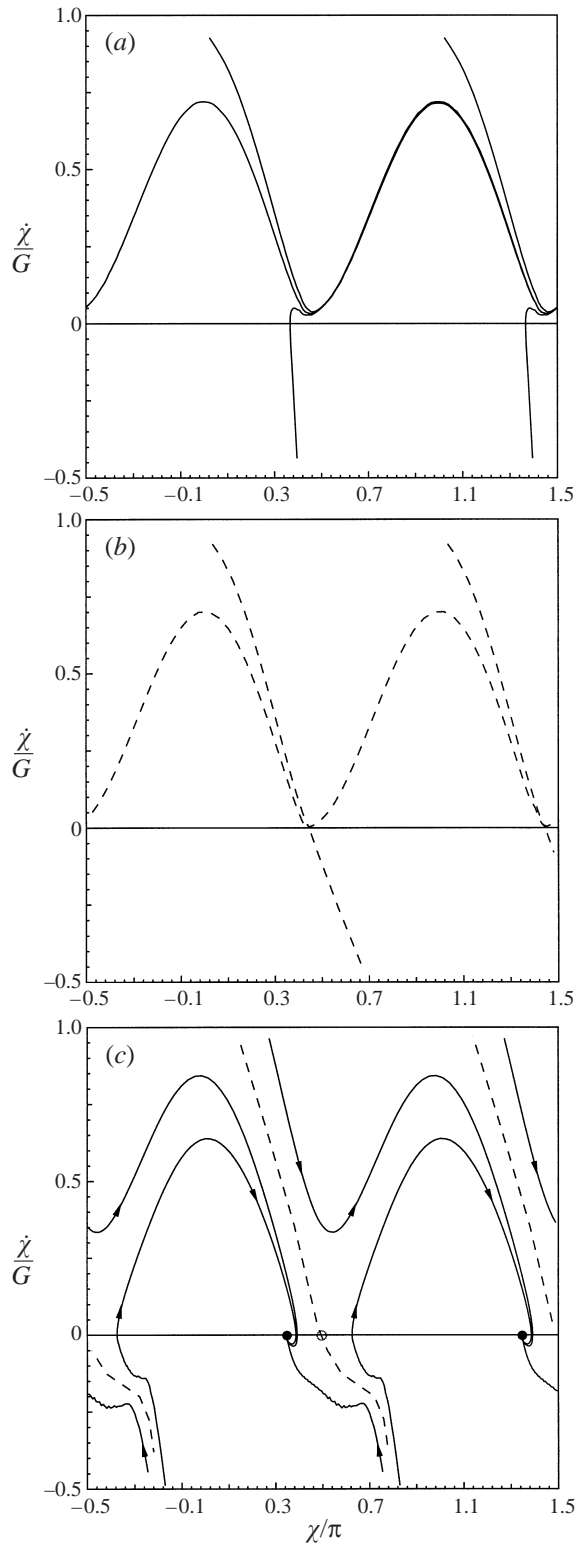


FIGURE 14. For caption see facing page.

in T . In other words, T is very sensitive to the minimum value of the rate of rotation near the point of transition.

5. The effect of density ratio on the dynamics

All of the analyses in the previous section treat the solid particle density ρ_s equal to the fluid density, ρ_f . The discussion in this section will be centred on the universality of the scaling law (12), i.e. the effect of Stokes number, or the ratio of densities, $\alpha = \rho_s/\rho_f$, on the scaling law.

Numerical results, of which a few are shown in figure 16, display the structure of the parameter space. The parameter space is divided into two regions by a dashed line. The symbol \bigcirc in this figure represents the stationary state, while $+$ represents the rotation state. The transition between the stationary state and the rotation state takes place at the critical Reynolds number, Re_c , corresponding to the dashed line in figure 16. Results for $\alpha = 1$, obtained in the previous section, are included in this figure.

In order to see the effect of the density ratio on the dynamics, the temporal variations of the rotation rate for a fixed value of Reynolds number and different values of α are compared. Results for $Re = 10$ are summarized in figure 17. It is found that on increasing the density ratio, the initial transient time becomes longer, and the fluctuation amplitude of angular velocity becomes smaller. This is a direct consequence of the solid particle inertia. As $\alpha \rightarrow \infty$ one may expect that the ellipse will rotate indefinitely with its initial rate of rotation. With decreasing the density ratio, the minimum of $\dot{\chi}/G$ decreases. When the density ratio is 100, 20, 1.0 and 0.25, the minimum value of the rotation rate, $\dot{\chi}/G$, is 0.40, 0.29, 0.09, and 0.085, respectively. By extrapolation, it is estimated that the minimum of $\dot{\chi}/G$ is about 0.083 when $\alpha \rightarrow 0$. When $Re = 10$ the system always approaches a time-periodic rotation state.

For $Re = 50$, the temporal variations of the rotation rate are also calculated as a function of α . If $\alpha \geq 3$, the minimum of $\dot{\chi}/G$ will always be positive, and the ellipse will rotate forever in a time-periodic manner. If $\alpha \leq 2$, however, the system will approach a steady state, as shown in figure 18. At some value of α , say α_c , between 2 and 3 the minimum of $\dot{\chi}/G$ will be zero. The minimum of $\dot{\chi}/G$ decreases when α decreases, and a straight line fit similar to (9) will be obtained. Based on similar reasoning to that presented in the previous section, the oscillation period scales with the density ratio according to the same $-1/2$ exponent, that is

$$GT = C(\alpha - \alpha_c)^{-1/2},$$

where C is a constant. The exponent, $-1/2$, representing the general scaling law remains the same.

It is clear from the results presented in this section that the critical Reynolds number, Re_c , is dependent on the density ratio, α . From the results summarized in figure 16, it is concluded that the critical Reynolds number increases with α .

In order to verify the universality of the exponent a calculation along different

FIGURE 14. The trajectories of the ellipse in phase-space. (a) $Re = 20 < Re_c$, (b) $Re = Re_c$, and (c) $Re = 100 > Re_c$. Solid lines are obtained by computational simulation, while dashed lines are drawn based on our knowledge of the dynamical behaviour of the system. The open and closed circles in (c) correspond to the stable and unstable nodes shown, respectively, in figure 12.

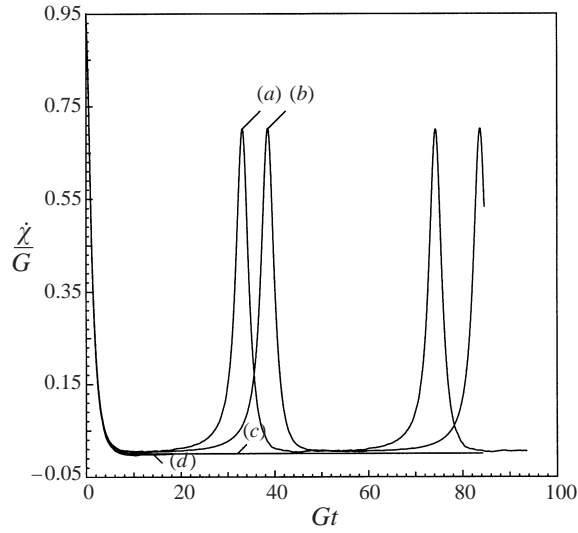


FIGURE 15. Comparison of the results of simulations with different size systems. Two sizes of systems, 1600×320 and 3200×640 , are calculated. (a) 1600×320 , $Re = 28$; (b) 3200×640 , $Re = 28$; (c) 1600×320 , $Re = 30$; (d) 3200×640 , $Re = 30$.

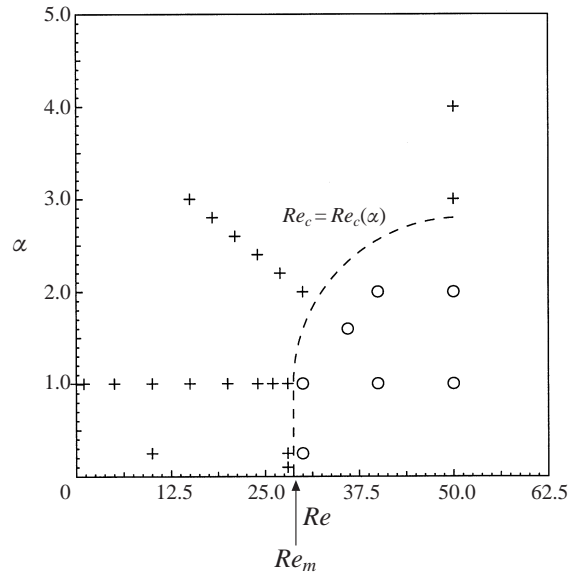


FIGURE 16. The transition boundary from a time-periodic state (+) to a steady state (O) in the density ratio–Reynolds number (α, Re) parameter space. The critical Reynolds number varies with density (i.e. $Re_c = Re_c(\alpha)$) where in the limit $Re_m = \lim_{\alpha \rightarrow 0} Re_c$. The initial orientation is $\chi_{initial} = 0$.

paths in parameter space is carried out. The line

$$\alpha = 4 - \frac{Re}{15} \tag{17}$$

is chosen arbitrarily as an example, where both parameters, Re and α , vary. The points along this line are shown in figure 16 as the inclined set of points. Although the density ratio is different for every point in figure 19, the period of the particle

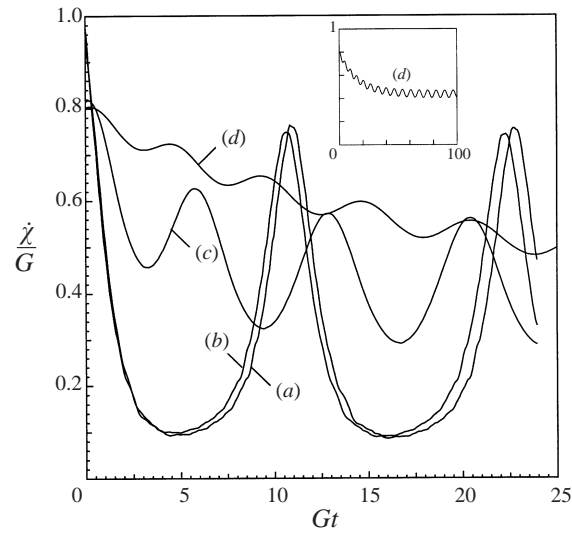


FIGURE 17. Simulation for $Re = 10$ with different values of the solid-to-fluid density ratio. (a) $\alpha = 0.25$; (b) $\alpha = 1.0$; (c) $\alpha = 20$; (d) $\alpha = 100$.

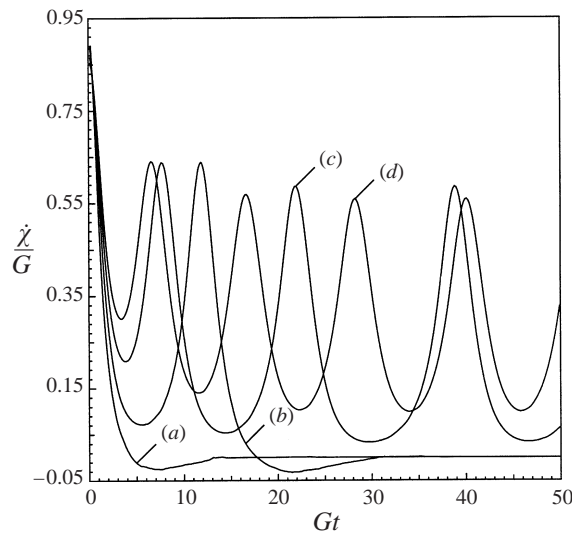


FIGURE 18. Simulation for $Re = 50$ with different values of the solid-to-fluid density ratio. (a) $\alpha = 1.0$; (b) $\alpha = 2$; (c) $\alpha = 3$; and (d) $\alpha = 4$.

rotation is given by (12) with $C = 106$ and $Re_c = 34.5$. From all of the above analyses it is concluded that the exponent $-1/2$ in the scaling law (12) is universal, independent of any details in the system. The reason is simple: the transition is through a saddle-node bifurcation (also known as tangent bifurcation) based on the system dynamics prior to and after the critical point. The critical exponent, $-1/2$, in the scaling law (12) is universal for every saddle-node bifurcation phenomenon (Lichtenberg & Lieberman 1992). The computational results from this study reveal that the transition is through a saddle-node bifurcation when a particle is suspended in shear flow. From this results, one can immediately generalize the scaling to any

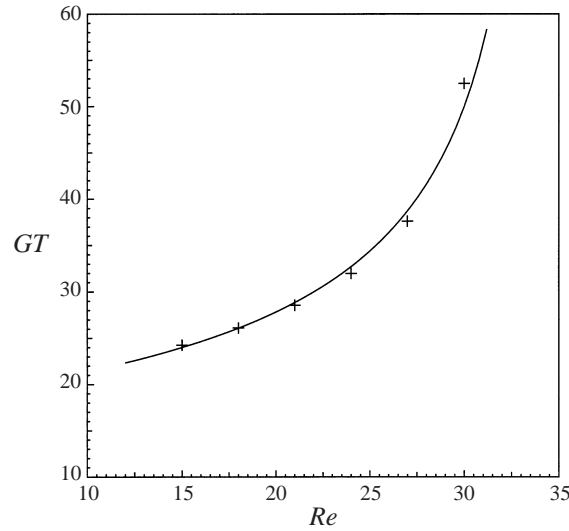


FIGURE 19. Along the line $\alpha = 4 - Re/15$ in parameter space the period of the motion of the ellipse follows the same scaling law as that in figure 10. Constants $C = 106$ and $Re_c = 34.5$ are used to fit the simulation results.

parameter, p , in the system (e.g. Re and α) which can lead to this transition. In other words, in general, the period of time-periodic flow or the rotation of the solid particle in the shear flow varies as

$$|p - p_c|^{-1/2},$$

where p_c is the critical value of the parameter p where the transition takes place.

6. A three-dimensional particle: ellipsoid in shear flow

The results presented in the previous section cover the dynamics of circular and elliptical cylinders in two-dimensional shear flow. In this section, a neutrally buoyant three-dimensional particle, an ellipsoid with semi-axes $a = b = 2c$ (oblate spheroid) in shear flow is considered. The axis of rotation is always the x -axis. At $Re = 0$, in the absence of inertia, the trajectories of two-dimensional and three-dimensional particles in two-dimensional shear flow are identical, as presented by Jeffery's solutions in (2) and (3). However, at $Re > 0$, the particle trajectories are no longer the same. Therefore, it is necessary to examine the dynamics of a three-dimensional particle and the difference with the two-dimensional cases presented above. The computational analysis of the particle motion in the range of Reynolds numbers 5 to 90 is presented in figures 20 to 22.

In a shear flow with a given shear rate, G , and fluid viscosity, ν , the particle Reynolds number, as defined here, is given by $4Gb^2/\nu$. A three-dimensional ellipsoid of a major semi-axis b can be constructed from infinite slices of elliptical cylinders with infinitesimal thickness and major semi-axis in the range of 0 to b . Hence we conjecture that the rate of rotation of the ellipsoid at some Reynolds number, say Re , should be in between the rate of rotation of the two-dimensional cases at Reynolds number 0 and Re . This analysis may help in understanding the dynamics of a three-dimensional ellipsoid in shear flow. As an example, as shown in figure 20, the rate of rotation of the ellipsoid at $Re = 5$ is in between the rate of rotation of the

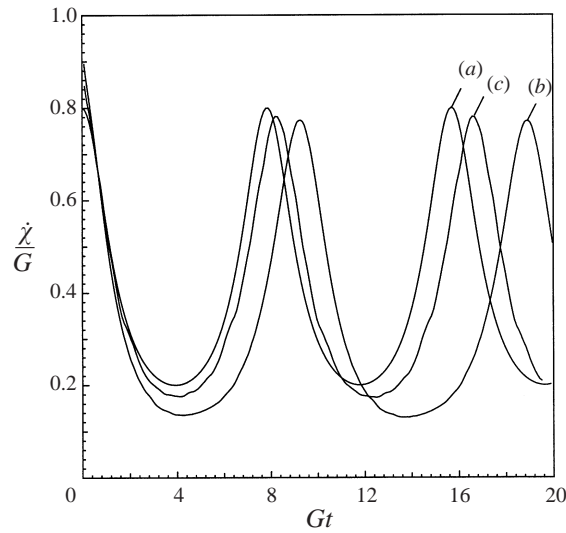


FIGURE 20. Comparison of the results of simulation between two-dimensional and three-dimensional systems. (a) two-dimensional particle (ellipse) or three-dimensional particle (ellipsoid) with $Re = 0$; (b) two-dimensional particle with $Re = 5.0$; (c) three-dimensional particle (ellipsoid) with $Re = 5.0$.

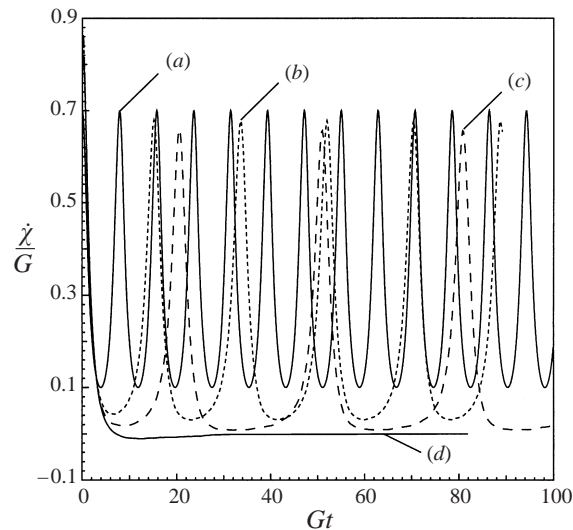


FIGURE 21. Three-dimensional simulation for $\alpha = 1$ with different values of Reynolds numbers. (a) $Re = 0$ (analytical results); (b) $Re = 50$; (c) $Re = 70$; (d) $Re = 90$.

two-dimensional cases at $Re = 0$ and 5. In other words, the deviation of the rotation rate for a three-dimensional ellipsoid at a Reynolds number, $Re > 0$, is smaller than that for a two-dimensional elliptical cylinder at the same Reynolds number. In §4, it is shown that the computational results at $Re = 0.08$ are in good agreement with Jeffery's solution, (2) and (3). For three-dimensional particles, agreement with Jeffery's solution is better than the two-dimensional case at a small Reynolds number.

The rate of rotation at $Re = 50, 70$, and 90 is compared in figure 21 to the asymptotic solution at $Re = 0$. Similarly to the two-dimensional case, the period

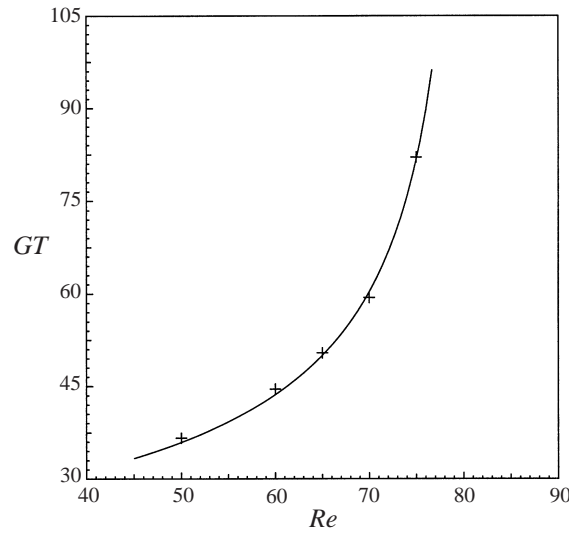


FIGURE 22. The period of the motion of the ellipsoid increases to infinity as the Reynolds number goes to the critical value. The curve in the figure represents equation (12) with $C = 200$ and $Re_c = 81$, which is in good agreement with the simulation results.

of rotation increases with the Reynolds number, approaching infinity at a critical Reynolds number, Re_c . The transition from time-periodic to steady state in the three-dimensional case, considered here, occurs at $Re_c = 81$. The critical Reynolds number for the three-dimensional case is higher than that for the two-dimensional case, consistent with the conjecture in the last paragraph. Application of the scaling law, presented in (12), with $C = 200$ provides a good fit to the rotation period of the ellipsoid from $Re = 50$ to $Re = 81$, as shown in figure 22. Again, the details of the case considered do not make a difference in the functional dependence of the scaling principle.

The computational domain for three-dimensional simulations is $40 \times 200 \times 80$ lattice nodes, and for various Reynolds numbers a combination of $8 \times 8 \times 4$ or $16 \times 16 \times 8$ lattice nodes is used to discretize the ellipsoid. The three-dimensional simulations are performed on the parallel processor system, SP2, with the Message Passing Interface (MPI) to minimize computational time. The total computational time (i.e. CPU + communication between processors + other overhead) for $Re = 70$ from $Gt = 0$ to 100 with 51 200 time steps using 16 processors is about 3.5 hours; that is about 0.2 s per time step. As indicated above, the computational time with the lattice-Boltzmann method does not depend on the Reynolds number. This method provides an effective tool for further analysis of particles suspended in fluid.

7. Summary of results

The purpose of the present work is to discuss the effect of inertia on the dynamics of solid particles suspended in shear flow. To date, only the motion of a circular cylinder, an elliptical cylinder, and an ellipsoid, suspended in fluid, has been investigated. Some general conclusions may be stated based on the limited results presented above.

Inertia has significant influence on the dynamics of solid particles suspended in fluid. In the Stokes flow regime, the dynamics, being linear, exhibit no transitions or qualitative change with the flow. At small particle Reynolds number, the symmetry in

the Stokes flow around the particle is disrupted and the particle behaviour deviated gradually with added inertia. In the case of a particle in simple shear flow, the influence of inertia is to gradually increase the rotation period, acting as an added mass.

For a circular cylinder suspended in shear flow, the influence of inertia on the dynamics of the solid particle has been discussed by other investigators (Robertson & Acrivos 1970; Kossack & Acrivos 1974; Poe & Acrivos 1975 and Zettner & Yoda 2000). The results from the present computational analysis of a circular cylinder agree well with the experiments. When the Reynolds number increases in value, the rotation rate, $\dot{\chi}/G$, decreases, and the distance from the stagnation point to the centre of the cylinder decreases. The effect of the solid walls confining the shear flow in a narrower channel is found to be significant. It results in a faster motion of the fluid near the moving walls, and it contributes a positive torque in favour of the rotation of the solid particle. At the same time, the confinement makes the recirculating flow in the centre region between the two walls exert a larger negative torque on the particle. The competition between these opposing torques influences the dynamics differently, depending on the value of the Reynolds number. At low Reynolds number, the existence of the walls suppresses the dimensionless rotation rate. The rate of rotation reaches a plateau depending on H/r when the Reynolds number is low enough. At high Reynolds number, the rotation rate of the circular cylinder increases as the distance between the walls decreases.

For an elliptical cylinder, and an ellipsoid, suspended in fluid, critical Reynolds numbers are found in the present investigation where the dynamics of the solid particle change significantly, and a new steady state appears. In the case presented in this paper, at the critical Reynolds number, the positive torque on the particle contributed by the shear layer is balanced by the negative contribution from the recirculating region of the fluid, and the upstream–downstream asymmetry in flow field changes the steady state from periodic to stationary, as shown in §4. The value of the critical Reynolds number is dependent on the solid-to-fluid density ratio, $\alpha = \rho_s/\rho_f$. The critical Reynolds number increases with the solid-to-fluid density ratio, as shown in figure 16.

The universal scaling law, (12), is the most interesting result in the present work. The transition from a time-periodic to a stationary state in a hydrodynamic system may be through various bifurcation mechanisms with different scaling characteristics. In this case, knowledge of the nature of bifurcation based on the system dynamics prior to and after the critical point of transition has provided the critical information leading to a universal scale. This universal scaling law, found and presented in this study, should not be confused with the non-universal scaling for a circular cylinder where no transition from one state to another has been shown to exist at finite Re . The computational results in §§4, 5, and 6 reveal that for the case of an elliptical cylinder or an ellipsoid suspended in shear flow, there is a transition to steady state through a saddle-node bifurcation. However, there is no evidence showing that the scaling relation found numerically for the circular cylinder in an unconfined shear flow is through a tangent bifurcation or any kind of transition. In fact, for the elliptical cylinder or the ellipsoid, prior to the bifurcation (when $Re < Re_c$), the rotation rate varies in a periodic manner going through maximum and minimum values, while for the circular cylinder the rate is a constant. For the elliptical cylinder or the ellipsoid, the minimum of the rotation rate, $\dot{\chi}_{min}/G$, is linearly dependent on the Reynolds number, as shown in (9), while for the circular cylinder the rotation rate is not linearly dependent on the Reynolds number. The period of the rotation of the

elliptical cylinder or the ellipsoid is proportional to $(\dot{\chi}_{min}/G)^{-1/2}$, while the rotation period of the circular cylinder is proportional to $(\dot{\chi}/G)^{-1}$. For the elliptical cylinder or the ellipsoid, after the bifurcation, there are two fixed orientation angles in the system, where one is stable and the other is unstable. For circular cylinders, however, since $c/b = 1$, a stable orientation can never coexist with an unstable orientation in the system. Therefore, the exponent in the scaling law for the elliptical cylinder or the ellipsoid is universal, independent of any details of the system, such as the confinement of the channel, the density ratio, and the aspect ratio of the particle, while the exponent in the scaling relation for the circular cylinder at $Re \rightarrow \infty$ depends on the confinement H/b , and it is not universal.

8. Conclusions and hypotheses

There is very little information available in the literature on the influence of inertia on the behaviour of elliptical cylinders or ellipsoids in shear flow. In fact, the authors could only find the limited computations by Feng & Joseph (1995), which are in the low-inertia regions ($Re = 1.0$). As shown by Aidun *et al.* (1998), the impact of inertia on particle dynamics in shear flow is significant. They show that by increasing the Reynolds number, the motion of the elliptical body undergoes a major transition from time-periodic rotation to a time-independent stationary state. Further analyses, presented above, reveal the details of this transition, as well as a universal scaling law. The remainder of this section is devoted to broader conclusions from the results presented above.

Consider a solid particle placed in a shear flow. At $Re = 0$, the streamlines are fully attached (Jeffrey & Sherwood 1980), and therefore the torque on the particle is always positive forcing the particle to rotate, creating a time-periodic state. In the absence of inertia, the flow is steady state if the particle is a body of revolution and the axis of revolution is perpendicular to the plane of shear (from now on referred to as the *body of revolution*). Otherwise, the flow is time periodic with a single frequency determined by the rate of rotation of the particle. This is because at $Re = 0$, regardless of the shape of the particle, the streamlines are fully attached, although the region of closed streamlines extends to infinity (Cox, Zia & Mason 1968; Jeffrey & Sherwood 1980).

At $Re > 0$, however, the streamlines detach creating a region with flow recirculation, as shown in figure 3 and figure 11. The gross influence of the flow recirculation on the particle is to generate a negative torque and to decrease the net torque exerted by the main shear stream; this is true regardless of the particle shape. Let us now consider the influence of inertia in two cases: the first is a particle with an arbitrary shape, and the second is the special case of the *body of revolution*.

In the first case, the net torque on the particle varies with the orientation of the particle due to the location of the flow separation and the magnitude of the negative torque contributed by the recirculating streamlines on the particle. The rate of rotation varies in a periodic manner going through minimum and maximum values, accordingly.

The second case is considered to be an asymptotic limit of the first case. That is, as the relevant particle aspect ratio, β , approaches 1, then the particle becomes a *body of revolution*. With this view of the second case, we can think of the problem in general, where $\beta < 1$, and then consider the special case when $\beta \rightarrow 1$.

In the general case, the effect of the fluid inertia on the rotation of a particle in shear flow is to decrease the net torque on the particle through flow separation. We will now present a few hypotheses which outline the characteristics of the first

transition in the particle motion in shear flow, regardless of the particle shape or the particular specifications of the shear flow.

Hypotheses: (a) A solid object (with $\beta < 1$) in time-periodic motion in a shear field undergoes a transition from a time-periodic state to a stationary (steady) state at a critical particle Reynolds number, $Re = Re_c$, at a solid to fluid density ratio, α_c , where $Re_c = Re_c(\alpha)$, and $\lim_{\alpha \rightarrow 0} dRe_c/d\alpha = 0$, as shown by the dashed line in figure 16. (b) The transition from a time-periodic to a steady state is through a saddle-node (tangent) bifurcation. (c) The period of the time-periodic system (i.e. the period of rotation) near the transition is proportional to $(Re_c - Re)^{-1/2}$, $(\alpha - \alpha_c)^{-1/2}$, $|q - q_c|^{-1/2}$ (note: q is the shape parameter defined in (7)), and in general, $|p - p_c|^{-1/2}$, where p represents any parameter in the system where a saddle-node transition takes place at $p = p_c$. (d) Below a certain Reynolds number, Re_m , the particle motion, and consequently the flow, will remain time-periodic regardless of the particle density ratio. (e) As the shape factor, β , approaches 1, the saddle-node bifurcation ceases to exist and the universal scaling is no longer valid.

We further conjecture that because the hypotheses presented above are independent of the particular shape of the particle or the profile of the shear field, in principle, the same is true for laminar shear or mean turbulent shear, as long as the axis of rotation of the particle is perpendicular to the plane of shear. In fact, as long as the particle is in a time-periodic rotation and the effect of fluid inertia is flow separation and, consequently, negative torque on the particle, the transition will be through a saddle-node (or tangent) bifurcation. This can be understood by examining the variation of the net torque with particle orientation, presented in figure 12. At $Re = Re_c$, there is only one particle orientation where the net torque is zero (point of tangent). As Re increases, this point bifurcates into two points of intersection representing stable and unstable fixed points through a saddle-node transition.

We acknowledge helpful discussions with Dr J. Feng, Dr J. Morris, and Dr M. Yoda. This study has been supported in part by the National Science Foundation through grant CTS-9258667 and by industrial matching contributions. The three-dimensional computations were conducted using the parallel supercomputer system, SP2, at the Cornell Theory Center which is funded by the National Science Foundation and New York State.

REFERENCES

- AIDUN, C. K. & DING, E. 1997 Computational analysis of suspensions in high shear blade coaters. *Euromech 367, 'Fluid Mechanics of Coating Processes', Proc. Second European Coating Symposium (ECS '97), 22–25 July, 1997* (ed. P. Bourgin). Université Louis Pasteur, France, p. 63.
- AIDUN, C. K. & LU, Y. 1995 Lattice Boltzmann simulation of solid particles suspended in fluid. *J. Statist. Phys.* **81**, 49.
- AIDUN, C. K., LU, Y. & DING, E. 1997 Dynamic simulation of particles suspended in fluid. *1997 ASME Fluids Engineering Division Summer Meeting (FEDSM '97), June 22–26*.
- AIDUN, C. K., LU, Y. & DING, E. 1998 Direct analysis of particulate suspensions with inertia using the discrete Boltzmann equation. *J. Fluid Mech.* **373**, 287.
- BOSSIS, G. & BRADY, J. F. 1984 Dynamic simulation of sheared suspensions. *J. Chem. Phys.* **80**, 5141.
- BRADY, J. F. & BOSSIS, G. 1988 Stokesian Dynamics. *Ann. Rev. Fluid Mech.* **20**, 111.
- BRETHERTON, F. P. 1961 Slow viscous motion round a cylinder in a simple shear. *J. Fluid Mech.* **12**, 591.
- COX, R. G., ZIA, L. Y. & MASON, S. G. 1968 Particle motions in sheared suspensions, XXV, Streamlines around cylinders and spheres. *J. Colloid Interface Sci.* **27**, 7.

- FENG, J. & JOSEPH, D. D. 1995 The unsteady motion of solid bodies in creeping flows. *J. Fluid Mech.* **303**, 83.
- GOLDSMITH, H. L. & MASON, S. G. 1961 Particle motions in sheared suspensions. 13. The spin and rotation of disks. *J. Fluid Mech.* **12**, 88.
- JEFFREY, D. J. & SHERWOOD, J. D. 1980 Streamline patterns and eddies in low-Reynolds-number flow. *J. Fluid Mech.* **96**, 315.
- JEFFERY, G. B. 1922 The motion of ellipsoidal particles immersed in a viscous fluid. *Proc. R. Soc. Lond. A* **102**, 161.
- KOSSACK, C. A. & ACRIVOS, A. 1974 Steady simple flow past a circular cylinder at moderate Reynolds numbers: a numerical solution. *J. Fluid Mech.* **66**, 353.
- LADD, A. J. C. 1994a Numerical simulations of particulate suspensions via a discretized Boltzmann equation. Part 1. Theoretical foundation. *J. Fluid Mech.* **271**, 285.
- LADD, A. J. C. 1994b Numerical simulations of particulate suspensions via a discretized Boltzmann equation. Part 2. Numerical results. *J. Fluid Mech.* **271**, 311.
- LADD, A. J. C. 1996 Hydrodynamic screening in sedimenting suspensions of non-Brownian spheres. *Phys. Rev. Lett.* **76**, 1392.
- LADD, A. J. C. 1997 Sedimentation of homogeneous suspensions of non-Brownian spheres. *Phys. Fluids* **9**, 491.
- LEAL, L. G. 1980 Particle motions in a viscous fluid. *Ann. Rev. Fluid Mech.* **12**, 435.
- LICHTENBERG, A. J. & LIEBERMAN, M. A. 1992 *Regular and Chaotic Dynamics*. Applied Mathematical Sciences, vol. 38 (ed. F. John, J. E. Marsden & L. Sirovich). Springer.
- MCMANARA, G. R. & ZANETTI, G. 1988 Use of the Boltzmann equation to simulate lattice-gas automata. *Phys. Rev. Lett.* **61**, 2332.
- POE, G. G. & ACRIVOS, A. 1975 Closed-streamline flows past rotating single cylinders and spheres: inertia effect. *J. Fluid Mech.* **72**, 605.
- ROBERTSON, C. R. & ACRIVOS, A. 1970 Low Reynolds number shear flow past a rotating circular cylinder. Part 1. Momentum transfer. *J. Fluid Mech.* **40**, 685.
- ZETTNER, C. M. & YODA, M. 2000 The circular cylinder in simple shear at moderate Reynolds numbers: an experimental study. *Expts. Fluids* (to appear).